

Experimental aspects of flux expulsion in type-II superconductors

O. B. Hyun*

Electromagnetic Technology Division, National Institute of Standards and Technology, Boulder, Colorado 80303

(Received 29 December 1992)

Experimental aspects of flux expulsion in Nb_3Sn and $\text{YBa}_2\text{Cu}_3\text{O}_7$ type-II superconductors are presented. There is a clear distinction in magnetization between field-cooled measured-upon-cooling (FCC) and field-cooled measured-upon-warming (FCW) results. This thermal hysteresis, predicted in the temperature-dependent critical-state model at low fields by Clem and Hao, was observed for measuring fields up to about 0.5 T. The model explains the observation of increases in diamagnetism after field cooling and thermal cycling. The thermal hysteresis, together with weak links, accounts for the occurrence of a negative peak in FCW magnetization. The FCC-FCW bifurcation observed for a 0.1 mT field down to 5 K might imply that flux lines are not completely frozen below T_{c1} , the temperature at which the lower critical field is equal to the measuring field, but are expelled from the sample even in the Meissner state.

I. INTRODUCTION

The temperature-dependent magnetization $M(T)$ of superconductors is usually measured in the zero-field-cooled (ZFC) mode, which produces screening diamagnetism, and the field-cooled (FC) mode, which produces thermodynamic flux expulsion. In thermal equilibrium, in the absence of flux pinning, the magnetization would be reversible at all temperatures, and there would be no difference between ZFC and FC data. Flux pinning interferes with both inward and outward flux motion, so diamagnetism becomes greater for ZFC and smaller for FC than that for the equilibrium state. Based on the critical-state model,^{1,2} Krusin-Elbaum *et al.*^{3,4} and Matsushita *et al.*^{5,6} calculated the flux expulsion including the internal flux profiles for the ZFC and FCC modes, and Clem and Hao⁷ calculated it for the FCW mode. According to the model, there exists flux freezing upon cooling, and flux relaxation upon warming after field cooling (FC), which leads to hysteretic magnetization between FCC and FCW, depending upon the pinning strength. For the low pinning case, there is negligible flux freezing, so FCC and FCW magnetization are nearly the same. For the high pinning case, the critical state exists only in a certain depth from the sample edge, while the inner core maintains the flux lines frozen upon cooling. When the sample is warmed, the frozen flux lines relax and move toward the region with lower flux density, while vortices move in from the outside through the edge. This flux relaxation hinders magnetization recovery, yielding greater diamagnetism for the FCW than for the FCC case. Although the hysteresis was predicted for applied field H below the lower critical field at zero temperature $H_{c1}(0)$, the same model should apply for fields higher than $H_{c1}(0)$. When $H \gg H_{c1}(0)$, however, the difference between FCC and FCW magnetization becomes insignificant because either $M(T) \ll H$ or the critical current density J_c is low.

This study experimentally investigates flux expulsion in the type-II superconductors Nb_3Sn and $\text{YBa}_2\text{Cu}_3\text{O}_7$.

First, we show that the temperature-dependent critical-state model adequately explains the magnetization as a function of temperature. Second, increases of diamagnetism upon thermal cycling after FC will be discussed as a direct result of flux freezing. Third, the model will be used to explain the occurrence of a negative peak⁸ in the FCW data of some polycrystalline samples as an effect of the thermal hysteresis in the grains, together with weak links between the grains. There is a numerical discrepancy between the model and the data, however. This is ascribed to an inappropriate model for the temperature dependence of the critical current density $J_c(T)$, the reversible magnetization $M_r(T)$, the surface-barrier contribution, and possible flux expulsion in the Meissner state.

II. EXPERIMENT

The samples used in this study are polycrystalline and powdered Nb_3Sn , and powdered $\text{YBa}_2\text{Cu}_3\text{O}_7$ (Y 1:2:3) grain-oriented in epoxy. For Y 1:2:3, H was applied parallel to the c axis. The magnetization data were taken in a commercial superconducting quantum interference device (SQUID) magnetometer equipped with a 5.5 T superconducting magnet. Between 5 and 30 K, the magnetometer ramps the temperature with 0.1 K overshoot. For temperatures between 60 and 90 K, the temperature ramp was controlled so that the apparent overshoot was less than 0.3 K for increasing temperature and 1 K for decreasing temperature. The actual temperature of the powder-epoxy composite specimen took more than 1 h to reach equilibrium due to its relatively large heat capacity. Since the temperature ramp was only about 3 K/h for 1-K steps near 80 K, the difference between apparent and equilibrium temperatures would be small compared to the thermal hysteresis of $M(T)$ of the grains. For this reason, any error due to temperature disequilibrium can be neglected. For the critical-state measurement, powder samples were used to eliminate the weak-link effect, and the polycrystalline sample was used to observe it.

III. RESULTS

A. Temperature-dependent magnetization

The magnetic-flux profile in the critical state for an infinite slab superconductor is given by⁷

$$B(x) = \mu_0 [H + M_r(T) \pm J_c(T)(x - D/2)], \quad (1)$$

$$0 \leq x \leq D/2,$$

where M_r is the reversible magnetization, which can be calculated from the free energy of the flux-line lattice in the thermodynamic equilibrium state.⁹ The coordinate x runs from 0 (sample center) to $D/2$ (sample edge), where D is the sample width. The + sign preceding $J_c(T)$ is for ZFC and FCW processes, and the - sign is for the FCC process. Application of the model to calculate the internal flux profile requires appropriate knowledge of M_r , which is technically difficult to obtain because of flux pinning and the image force. Nevertheless, using $M_r(T) = -H_{c1}(T)$, a model fit was attempted with two parameters: $H_{c1}(0)$ and γ , defined as⁷

$$\gamma = \left[\frac{D}{2} \right] \frac{J'_c(T)}{H'_{c1}(T)}, \quad (2)$$

where the primes denote derivatives with respect to temperature. $H_{c1}(T)$ was assumed to be uniform in the sample,^{10,11} and this is approximately the case when the Ginzburg-Landau parameter $\kappa \gg 1$ and the upper critical field $H_{c2}(0) \gg H_{c1}(0)$, as in the present samples. In accordance with Ref. 7, for convenience in the calculation, we take $H_{c1} = H_{c1}(0)(1-t^2)$ and $J_c = J_c(0)(1-t^2)$, where $t = T/T_c$. Therefore, γ is temperature independent and is equal to $\gamma_0 = (\frac{1}{2}D)J_c(0)/H_{c1}(0)$. Assuming J_c is independent of local magnetic induction B , Eq. (1) can be written as

$$B(x) = \mu_0 H - \mu_0 H_{c1}(0) [(1-t^2) \mp \gamma_0(1-t^2)(x-1)], \quad (3)$$

$$0 \leq x \leq 1,$$

where the coordinate x is normalized to $D/2$. The magnetization calculation follows the procedures in Ref. 7:

$$\mu_0 M = \int_0^1 [B(x) - \mu_0 H] dx. \quad (4)$$

Magnetization for both FCC and FCW modes was calculated down to T_{c1} , the temperature at which $H = H_{c1}$. Below T_{c1} the sample is in the Meissner state and flux lines are assumed to be frozen. The model applies for samples having an infinite slab geometry, and clearly the Nb_3Sn and Y 1:2:3 powder samples do not satisfy this condition. Since we are more interested in the qualitative behavior of $M(T)$, rather than its precise values, the $M(T)$ data are normalized by the maximum value M_{\max} , which is considered to be the magnetization value in the full shielding state. Experimentally, magnetization at 5 K, $\mu_0 M_{\max}$, at $\mu_0 H = 10$ mT were -15.6 mT for powdered Nb_3Sn and -18.9 mT for Y 1:2:3. If these values reflect the demagnetizing factors, the factors would be approximately $\frac{1}{3}$ for powdered Nb_3Sn and $\frac{1}{2}$ for Y 1:2:3. Therefore, Nb_3Sn is more likely spherical grains,

and Y 1:2:3 is barlike grains perpendicular to H . A calculation of $M(T)$ in the cylindrical coordinate simply increases γ_0 by a factor of $\frac{3}{2}$ with slight changes in the values of $M(T)$.

Figure 1 shows magnetization data at an applied field $\mu_0 H = 10$ mT in ZFC, FCC, and FCW modes for Nb_3Sn powder. The calculated $M(T)$ is shown by the solid lines. The parameters used are $\mu_0 H_{c1}(0) = 24$ mT and $\gamma_0 = 1.1$. The gradual increase of diamagnetism at low temperatures is thought to be due to the change in penetration depth λ_L for the grains with temperature. The flux profiles for ZFC, FCC, and FCW modes at 16 K are shown in Fig. 1(b). In the FCC process, $B(x)$ is constant for $x \leq x_0 = 0.09$, and the critical state exists for $x_0 \leq x \leq 1$, where x_0 is the flux-freezing front measured from the center. These linear $B(x)$ lines are due to the simplified choices of $H_{c1}(t)$ and $J_c(t)$. More realistic functions would cause the $B(x)$ to curve.¹² The V-shaped minimum in the FCW process is at $x_0 = 0.80$ at 16 K. Figure 2 exhibits the magnetization data at $\mu_0 H = 10$ mT parallel to the c axis and the model fit (solid lines) for Y 1:2:3. The parameters used are $\mu_0 H_{c1}(0) = 25$ mT and $\gamma_0 = 1.2$. This value of γ_0 should not be used to estimate $J_c(0)$ because the specimen was not in the full critical state at temperatures below T_{c1} .

As indicated in the model, both specimens show clear distinctions between FCC and FCW data. To tell if there

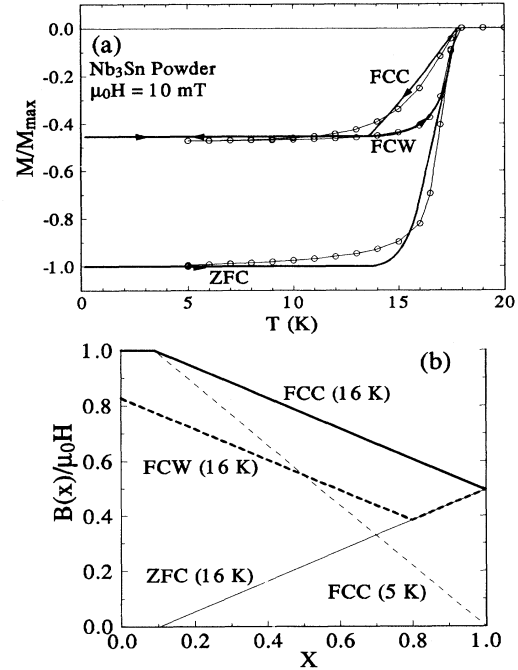


FIG. 1. (a) $M(T)$ for Nb_3Sn powder sample ($T_c = 18$ K) at 10 mT. The FCC data are clearly different from FCW data. The solid lines are the model-predicted curves with $\mu_0 H_{c1}(0) = 24$ mT and $\gamma_0 = 1.1$, according to Ref. 7. (b) Flux profiles at 16 K after ZFC (thin solid line), after FCC (thick solid line), and FCW (thick dashed line). The thin dashed line is at 5 K after FCC.

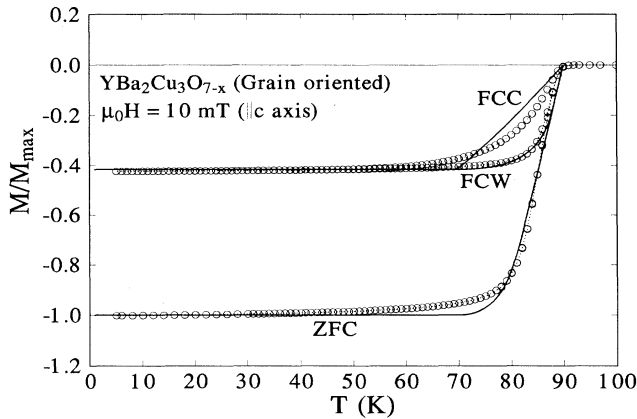


FIG. 2. Magnetization data for the $\text{YBa}_2\text{Cu}_3\text{O}_{7-x}$ grain-oriented sample at 10 mT parallel to the c axis. The solid line is the model fit with $\mu_0 H_{c1}(0) = 25$ mT and $\gamma_0 = 1.2$.

are flux-creep effects, magnetization was measured under a slow rate of temperature change. There were no visible differences in $M(T)$ between 3-h measurement and 9-h measurement from 18 K (FCC) to 18 K (FCW) via 5 K. This means that the thermal hysteresis in FCC and FCW is solely due to internal flux motion subject to the temperature-dependent critical-state model. This type of hysteresis was observed not only below $H_{c1}(0)$, but also in higher fields up to 0.5 T as shown in Fig. 3. At higher fields than 1 T, the hysteresis becomes insignificant although there is a distinction in flux profiles between FCC and FCW processes. Although the model predicts the basic properties, there are differences between the model and the experimental data, particularly in the value of $H_{c1}(T_{c1})$, at which FCW data splits from FCC data, and in slope of the $M(T)$ curves near T_c . These discrepancies and the interpretation of γ_0 are discussed further in the next section.

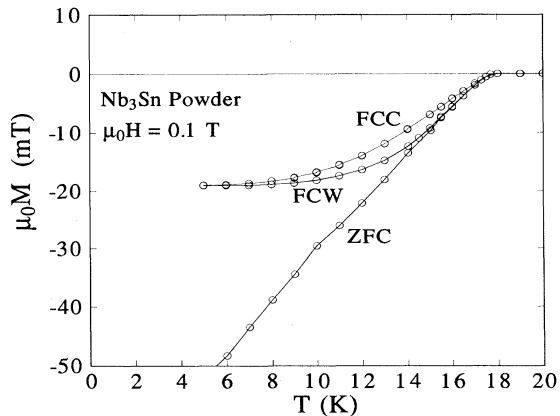


FIG. 3. Magnetization data for the Nb_3Sn powder sample at $\mu_0 H = 0.1$ T, which must be greater than $\mu_0 H_{c1}(0)$. At $\mu_0 H = 1$ T the hysteresis between FCC and FCW is negligible.

B. Diamagnetism increase by thermal cycling

In conjunction with the FCC-FCW bifurcation, we can expect that the diamagnetism can be increased if the temperature is cycled between $T_0 (= 5 \text{ K} < T_{c1})$ and $T_1 (= 16 \text{ K} < T_c)$ in an applied field $\mu_0 H = 10$ mT. When a superconductor is cooled in an applied field through T_c , the flux-line density for $x < x_0$ does not change, where x_0 is the flux-freezing front. The critical state exists only for $x > x_0$, and fluxons in this region move out in such a way that the flux profile becomes linear in x . When the sample is warmed, flux lines move in from the outside, while the frozen fluxons for $x < x_0$ simply move outward to fill the less congested region in the sample. The flux profiles at T_0 and T_1 are depicted by the thin solid line (A) and the dashed line (B), respectively, in the inset of Fig. 4. If the sample temperature is lowered from T_1 to T_0 again, the flux lines in the region $x < x_0$ freeze again. The critical state exists and flux lines move out for $x > x_0$, as in the case of the first FCC. Therefore, the flux-line density near the edge is almost the same as for the first cooling case, but it is much lower for $x < x_0$. Consequently, the total diamagnetic moment at T_0 increases as shown by the heavy solid line (C) in inset of Fig. 4. Repetition of the same thermal cycling continuously increases the diamagnetism. The rate of increase becomes smaller as thermal cycling goes on and finally saturates at some value between M_{ZFC} and the initial M_{FC} .

C. Negative peak in FCW

A negative peak in FCW magnetization was observed in a polycrystalline Y 1:2:3 sample which contains weak links. Since the negative peak disappears for a powder sample and for measurements with slow temperature change, it has been ascribed to the effect of weak links to-

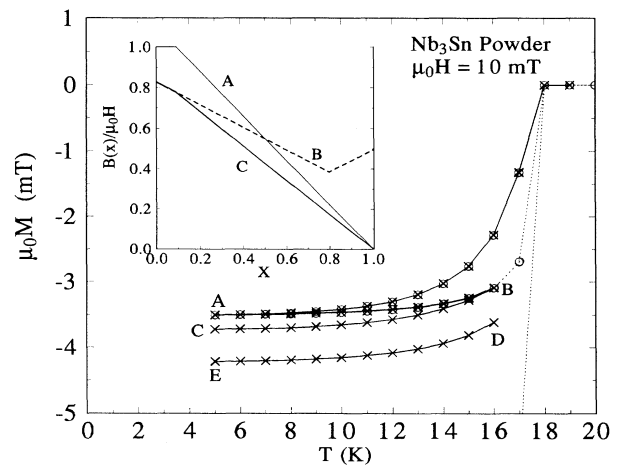


FIG. 4. Diamagnetism increase by thermal cycling after FCC. The inset is the consecutive flux profiles at $T_0 = 5$ K after first FCC (A: thin solid line), at $T_1 = 16$ K after warming (B: broken line), and at $T_0 = 5$ K after second FCC (C: thick solid line). The data D-E are after 15 cycles between 5 K and 16 K.

gether with strong magnetic relaxation.⁸ Without magnetic relaxation, the temperature-dependent critical-state model can explain the negative peak as a weak-link effect in conjunction with thermal hysteresis of the grains. When a sample is cooled through T_c in an applied field, the grains expel vortices. Most of the expelled vortices may be trapped in grain boundaries below some $T_w (< T_c)$, the temperature at which weak links connecting the grains become superconducting; diamagnetism becomes smaller than that without weak links. When temperature increases, the vortices penetrate into the grains from the grain boundaries as well as from outside the sample. Because of thermal hysteresis in flux expulsion between FCC and FCW for the grains, the grain boundaries cannot return all of the trapped vortices to the grains. Instead, the remaining vortices are released from the sample at T_w , resulting in an abrupt increase of diamagnetism. The increase of diamagnetism becomes gradual because T_w is not same for all weak links. Figure 5 shows the behavior in a porous polycrystalline Nb₃Sn sample at $\mu_0 H = 5$ mT. The negative peak is narrow and high, and the peak point is close to T_c for low applied field. This is likely so because most weak links are broken in a narrow region of temperature just below T_c . As the applied field increases, the peak becomes low and broad. Above 50 mT, no negative peak was observed because of small thermal hysteresis and nonuniform T_w . Cycling temperature between $T_0 (= 5$ K) and $T_w (= 16$ K) expels more vortices from the sample to reach the value of a powder sample, as shown by the extended FCC-FCW data (crosses) in Fig. 5. The negative peak disappears, and normal $M(T)$ behavior is seen for a powder sample made from the same polycrystal, clearly demonstrating the importance of grain boundaries in the occurrence of the negative peak. In general, such a negative peak is thought to occur for a magnetically porous sample, which has homogeneous weak links connecting them to the sample surface.

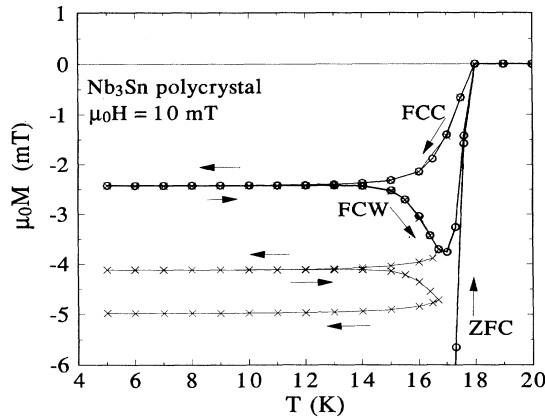


FIG. 5. Negative peak in $M(T)$ at 10 mT for a Nb₃Sn polycrystalline sample. A powder sample made from the same polycrystal has no negative peak as shown in Fig. 1. The flux expulsion at 5 K is much greater for the powder sample than for the polycrystal.

IV. DISCUSSION

As seen in Figs. 1 and 2, theoretical prediction of $M(T)$ with appropriate $H_{c1}(0)$ and γ_0 adequately describes the characteristics of the experimental data. There are some quantitative differences, however, between theory and data, particularly for the magnitude of $\Delta M(T) (\equiv |M_{\text{FCC}} - M_{\text{FCW}}|)$, stiffness of the transition near T_c , and the T_{c1} value for both Nb₃Sn and Y 1:2:3 samples. In addition, the determined $\mu_0 H_{c1}(0) = 24$ mT for Nb₃Sn and 25 mT for Y 1:2:3 are approximately correct, but $\gamma_0 = 1.1$ for Nb₃Sn and 1.2 for Y 1:2:3 are too small. Here, we discuss possible factors to be considered.

(i) The present choice of $H_{c1}(T)$ and $J_c(T)$ produces the flux expulsion ratio f_M ,⁷ where $f_M \equiv M_{\text{FCC}}/M_{\text{ZFC}}$ for $T \leq T_{c1}$:⁷

$$\begin{aligned} f_M &= 1 - \gamma_0/2, \quad \gamma_0 < 1, \\ &= 1/(2\gamma_0), \quad \gamma_0 \geq 1, \end{aligned} \quad (5)$$

For Y 1:2:3, f_M was 0.42 at 5 K at $\mu_0 H = 10$ mT; therefore $\gamma_0 = 1.2$. This value cannot be used to estimate J_c as mentioned above. It produces $J_c(0$ K, 10 mT) $= 8.8 \times 10^4$ A/cm², which is approximately 20 times smaller than $J_c(10$ K, 0 T) $= 2.1 \times 10^6$ A/cm² estimated from $M(H)$ hysteresis curve using the Bean model.^{1,2} $M(T)$ calculations for other geometries would not account for such a difference. In addition, f_M approaches 1 in the zero-field limit for La_{1-x}Sr_xCuO₄, Bi₂Sr₂CaCu₂O_y, and YBa₂Cu₃O_y.³⁻⁵ This means that both J_c and $\partial J_c/\partial T$ must vanish as temperature approaches T_c . The current model with $J_c \sim (1-t^2)$ does not satisfy this condition since $f_M < 1$ for finite γ_0 . Furthermore, the transition near T_c is sharper for the data than for the model, particularly for the ZFC and the FCC mode. These can be corrected by taking $J_c \sim (1-t)^n$ with $n > 1$ and $M_r \sim (1-t^2)$.¹² However, the functions $M_r \sim (1-t^2)$ and $J_c \sim (1-t^2)^n$ or $(1-t)^n$ did not quantitatively fit all of the ZFC, FCC, and FCW data well with reasonable values of γ_0 . An upturn in $H_{c1}(T)$ for Y 1:2:3 might be an indication of temperature dependence different from $(1-t^2)$.¹³

(ii) The model assumes that the magnetization, or the internal flux profile, is frozen for temperatures below T_{c1} . The current experiment could not prove this assumption. For Nb₃Sn the split between FCC and FCW was observed down to 5 K even at $\mu_0 H = 0.1$ mT, which is thought to be far below H_{c1} at 5 K. A change of λ_L with temperature does not explain this split because λ_L is almost constant except near T_c and the magnetization due to the change of λ_L is reversible. Experimental data show that $M(T)/H$ vs T for FCC and FCW modes at the applied field of 0.1 mT are almost the same as those at 10 mT, but with a sharper transition and greater $f_M (= 0.62$ at 0.1 mT) for the lower field. Measurement with slow temperature changes had no effect, which rules out a magnetic relaxation effect. Magnetization relaxation at 12 K for 3 h, which is longer than the temperature sweep time from 12 K (FCC) to 12 K (FCW), was at most 6% of $\Delta M(T)$ at 12 K. The Y 1:2:3 sample also showed a clear

distinction between M_{FCC} and M_{FCW} at 0.5 mT down to 5 K, although with smaller $\Delta M(T)$ than that of Nb_3Sn . This means that the fluxons may be expelled from the sample even below T_{c1} depending on the pinning strength.¹⁴ If the inner core can hold vortices for $T < T_{c1}$, the surface in the Meissner state might have transient vortices passing through it. If this is so, flux profiles for both FCC and FCW modes have significant changes from those in Fig. 1(b). The calculation of Eq. (4) extends to zero temperature, and there can be a flux-free zone near the surface below T_{c1} . For FCW, the flux-free zone may exist up to T_{c1} , causing constant M_{FCW} below T_{c1} . It will increase both $|M_{\text{FCC}}|$ and $|M_{\text{FCW}}|$, thereby causing a greater value for γ_0 than the present one for a given f_M . Further work is needed to understand the nature of the Meissner state associated with flux pinning.

(iii) The model assumes that flux pinning plays a dominant role in $M(T)$. This is not always the case, however. According to the critical-state model, $\Delta M(H) \equiv |M(H \text{ increasing}) - M(H \text{ decreasing})|$ is proportional to J_c and monotonously decreases as H increases. For powder samples, $\Delta M(H)$ often shows a narrow peak in the low-field region near the full penetration field, H^* . Both Nb_3Sn and Y 1:2:3 in this study show a peak in $\Delta M(H)$ at low-field region not only near T_c , but also at low temperatures. This peak should be distinguished from the field-induced magnetization increase called to as the peak effect¹⁵ at high fields. Chen and co-workers^{10,11} showed that such a peak can be predicted by the Bean-Livingston surface barrier,¹⁶⁻¹⁸ which is due to screening current and image forces acting on vortices. Since the bulk pinning may be considered as a barrier, or as the barrier itself, both bulk pinning and the surface barrier may produce qualitatively the same magnetic properties, as indicated by thermal hysteresis in FC magnetization and enhanced diamagnetism under surface heating.¹⁹⁻²² It is not easy to separate the individual components from the

data. Therefore, the surface barrier is not included in the $M(T)$ calculation, although the measured data would probably include it. This surface barrier is particularly important for low-field and weak-flux pinning. The height of the peak, however, was small compared to $\Delta M(H)$, meaning only a minor effect on the critical state. The surface barrier acts to increase the pinning strength; that is, actual γ_0 and f_M are smaller than the apparent values.

In summary, there is a clear distinction between magnetization of FCC and FCW for Nb_3Sn and Y 1:2:3. Thermal hysteresis was observed for $\mu_0 H$ up to 0.5 T, but insignificant above it. The temperature-dependent critical-state model was applied to describe magnetization $M(T)$ and to construct flux profiles $B(x)$ at low applied field. Using the simple functions $M_r \sim J_c \sim (1-t)^2$, the model predicted the basic nature of $M(T)$ for ZFC, FCC, and FCW. As a direct result of the thermal hysteresis, a diamagnetism increase under thermal cycling was observed. The model provides a good explanation for the occurrence of a negative peak in some polycrystalline samples. There are numerical differences between the data and the model fit for parameters such as $H_{c1}(T_{c1})$ and γ_0 . Several factors were discussed: using $J_c \sim (1-t)^n$, reinterpreting the Meissner state associated with flux pinning, and including a surface-barrier contribution. Modification of the model with these factors would give a better description of the temperature-dependent magnetization for applied fields both below and above $H_{c1}(0)$.

ACKNOWLEDGMENTS

I thank J. Clem and Z. Hao for communicating their results prior to publication, and R. B. Goldfarb for discussion on the measurement and a careful reading of the manuscript.

*Present address: International Superconductivity Research Center, 2-4-1-Mutsuno, Atsuta-Ku, Nagoya, 456 Japan.

¹C. P. Bean, Phys. Rev. Lett. **8**, 250 (1962).

²C. P. Bean, Rev. Mod. Phys. **36**, 33 (1964).

³L. Krusin-Elbaum, A. P. Malozemoff, D. C. Cronemeyer, and F. Holtzberg, Physica C **153-155**, 1469 (1988).

⁴L. Krusin-Elbaum, A. P. Malozemoff, D. C. Cronemeyer, F. Holtzberg, J. R. Clem, and Z. Hao, J. Appl. Phys. **67**, 4670 (1990).

⁵T. Matsushita, E. S. Otabe, T. Matsuno, M. Murakami, and K. Kitazawa, Physica C **170**, 375 (1990).

⁶K. Kitazawa, Y. Tomioka, T. Hasegawa, K. Kishio, M. Naito, T. Matsushita, I. Tanaka, and H. Kojima, Supercon. Sci. Technol. **4**, S35 (1991).

⁷J. R. Clem and Z. Hao (unpublished).

⁸T. Ishida, R. B. Goldfarb, S. Okayasu, and Y. Kazumata, Physica C **185-189**, 2515 (1991).

⁹A. L. Fetter and P. C. Hohenberg, *Superconductivity*, edited by R. D. Parks (Marcel Dekker, New York, 1969), Vol. 2, p. 830.

¹⁰D.-X. Chen and A. Sanchez, Phys. Rev. B **45**, 10 793 (1992).

¹¹D.-X. Chen, R. W. Cross, and A. Sanchez, Cryogenics **33**, 695 (1993).

¹²O. B. Hyun, Physica C **206**, 169 (1993).

¹³L. Burlachkov, Y. Yeshurun, M. Konczykowski, and F. Holtzberg, Phys. Rev. B **45**, 8193 (1992).

¹⁴T. Matsushita and K. Yamafuji, J. Phys. Soc. Jpn. **46**, 764 (1979).

¹⁵A. M. Campbell and J. E. Evetts, Adv. Phys. **21**, 199 (1972).

¹⁶C. P. Bean and J. D. Livingston, Phys. Rev. Lett. **12**, 14 (1964).

¹⁷M. Konczykowski, L. I. Burlachkov, Y. Yeshurun, and F. Holtzberg, Phys. Rev. B **43**, 13 707 (1991).

¹⁸J. R. Clem, J. Appl. Phys. **50**, 3518 (1979).

¹⁹M. A. R. LeBlanc, D. J. Griffiths, and H. G. Mattes, Appl. Phys. Lett. **11**, 143 (1967).

²⁰M. A. R. LeBlanc, D. J. Griffiths, and B. C. Belanger, Phys. Rev. Lett. **18**, 844 (1967).

²¹V. N. Kopylov, A. E. Koshelev, I. F. Schegolev, and T. G. Tognidze, Physica C **170**, 291 (1990).

²²R. B. Flippen, Phys. Lett. **24A**, 588 (1967).